# STRESS MEASUREMENTS IN A ROUGH WALL CHANNEL FLOW USING A VARIABLE ANGLE METHOD OF CALIBRATION FOR X-PROBES

**O.M. Bakken and P.-Å. Krogstad**
Dept. of Energy and Process Engineering
Norwegian University of Science and Technology
Kolbjoern Hejes v. 2, N-7491 Trondheim, Norway
ole.m.bakken@mtf.ntnu.no, per.a.krogstad@mtf.ntnu.no

## ABSTRACT

A comparison between the turbulent flows in a smooth and two different rough wall channels is reported. It is demonstrated that even though the outer layer may appear to be unaffected by the surface conditions, since the mean velocity defect profiles are very similar, modifications to the turbulent stresses as far out as $y/h \approx 0.3$ are found. Closer to the wall the contributions from the fourth quadrant are found to be much more dominant in the rough cases than over the smooth wall, confirming earlier findings that surface roughness tends to stimulate sweep type of motions. A velocity dependent effective angle method for the calibration of yaw-response of hot-wire X-probes at low velocities is presented. Comparisons with DNS (Moser *et al.*, 1999) show that this approach significantly improves estimates of Reynolds stresses at low velocities compared to the conventional method assuming a fixed effective angle.

## INTRODUCTION

Flows over rough surfaces play an important role in industry. Very few industrial processes are found in hydraulically smooth pipes. Townsend's (1976) similarity hypothesis propose that, outside the roughness sublayer ($\simeq 5$ times the roughness height, $k$) the flow is independent of wall roughness at sufficiently high $Re = \overline{U}_c h/\nu$ (based on centreline velocity $\overline{U}_c$, channel half height $h$ and the kinematic viscosity, $\nu$). An implication of this hypothesis is that outside the roughness sublayer the Reynolds stresses normalized by the friction velocity, $u_\tau$, are unaffected by the roughness. Krogstad *et al.* (1992) and later Krogstad and Antonia (1999), have questioned this assumption on the basis of differences observed in measurements over smooth and rough wall boundary layers. In a boundary layer, $u_\tau$ is deduced from the velocity measurements, which may contain considerable uncertainty. The present results are therefore obtained in a channel flow, where $u_\tau$ may be extracted more accurately from the measured longitudinal static pressure gradient or the known shear stress distribution.

The present study investigates the effects of surface roughness on the Reynolds stresses over two different roughness geometries for $12000 < Re < 70000$. Here only measurements for $Re \simeq 12000$ are shown. Measurements for the smooth wall channel are compared with DNS of Moser *et al.* (1999). Results from their $Re \simeq 12400$ simulation suggest that this is sufficiently high to be free from most low-$Re$-number effects.

## EXPERIMENTAL DETAILS

The experiments were performed in an open return wind tunnel with a working section consisting of two parallel plates which form a 2-D rectangular channel. The test section is 5 m long, with an inlet area of 1.35 m x 0.10 m. Reference measurements were first made in the smooth case. In the case of the first rough surface, the roof and floor were covered with square bars 1.7 x 1.7 mm spanning the width of the section. This corresponds to a ratio between the roughness height, k, and channel half height, h, of 0.034. The centreline spacing was 8 times the width of the bars, making it a $k$-type roughness. According to Furuya *et al.* (1976) this roughness spacing creates the largest effect on the mean velocity profile. The second rough surface consisted of 1.5 mm thick perforated plates covering both roof and floor. The perforation consisted of 10 × 10 mm square holes arrayed in a squared pattern with a centre spacing of 12 mm giving an openness ratio of about 83 percent.

The measurements were taken at a bulk velocity of about $\overline{U} = 4$ m/s for all three flows. Mean velocity and Reynolds stress data ($\overline{u^{+2}}, \overline{v^{+2}}, \overline{w^{+2}}, -\overline{u^+v^+}, \overline{u^+w^+}$, where $u$, $v$ and $w$ are fluctuations in the streamwise, wall normal and spanwise directions respectively and superscript + denotes normalization with $u_\tau$) were obtained using purpose made 2.5 $\mu$m diameter single-, X- and UW-wire probes (where X-wire probes are used for measurements of $u$ and $v$ and UW-wire probes are used for measurements of $u$ and $w$). As expected for two-dimensional flows $\overline{u^+w^+}$ was very close to zero and will not be presented. For all cases about 900 000 data were acquired to a PC. The filter frequency of the low-pass filter was adjusted for each surface after spectral investigation to closely match the highest Kolmogorov frequency in the flow. The flow along the roof and floor were both tripped at the inlet by a 3 mm diameter rod followed by a 12 cm strip of No. 40 grit sandpaper, both spanning the width of the section.

For the determination of $u_\tau$, two different methods have been used: (i) Measurement of the static pressure gradient in the streamwise direction, $dP/dx$. (ii) Calculation of $u_\tau$ from a least squares fit of $-\overline{uv}$ to the estimated outer layer total shear stress. For measurements of $dP/dx$ the test section is fitted with pressure taps with 20 cm spacing along the centreline. Additional taps are fitted off centre for rough two-dimensionality checks. For the rough cases the sidewalls were also fitted with pressure taps to eliminate disturbances from the roughness elements. In fully developed channel flow the total shear stress, $\tau^+_{total} = 1 - \frac{y^+}{h^+} = \frac{dU^+}{dy^+} - \overline{u^+v^+}$ is a straight line. A collapse of the measured shear stress outside of the region affected by viscosity onto this line is then a verification of the estimated $u_\tau$. For the higher $Re$ investigated the pressure drop was sufficient to obtain reliable estimates of $u_\tau$. $u_\tau$ from the pressure drop and the shear stress profiles for these $Re$ differed by less than 1 % for all surfaces. For the

lower $Re$ the pressure drop was only of the order of 2-10 $Pa$ for the 4 m length of the channel used for pressure measurements, thus causing higher measurement uncertainties. In the smooth case $u_\tau$ from the pressure gradient had to be adjusted by up to 8 % to ensure that the mean velocity profile agreed with results from DNS. This method compared to within 1 % with $u_\tau$ calculated from the shear stress profiles. For single- and UW-wire measurements the confirmation of $u_\tau$ was done by inspecting the mean velocity profiles. In the rough cases $u_\tau$ was calculated entirely from the shear stress profiles. Because of the shift in the mean velocity profile, another method had to be used in the rough cases for the confirmation of $u_\tau$ for single- and UW-wire measurements. Results from the smooth case showed complete collapse of the $\overline{u^{+2}}$ profiles in the outer layer ($y/h > 0.2$) measured with single-, X- and UW-wire at similar $Re$. In the rough cases the collapse of the $\overline{u^{+2}}$ profiles in the outer layer could then be used to estimate $u_\tau$ for the single- and UW-wire measurements.

The present study is part of a project comparing wind tunnel experiments with results from DNS. To match the low Reynolds numbers from the DNS it was necessary to decrease the flow speeds in the wind tunnel to a centreline velocity of 2 m/s. Preliminary results (Bakken and Krogstad, 2001) showed significant deviations in $\overline{v^{+2}}$ and $\overline{w^{+2}}$ in the measured smooth wall data at low velocities compared with DNS at the same $Re$. This led to an investigation of calibration procedures for the X-wire probes. Three methods for calibrating the yaw response are compared. (i) A yaw calibration is performed using a constant velocity to determine an average single effective angle. Such an approach is given by Bradshaw (1971, p.121). This method has been used consistently by our group and was the basis for the preliminary results. (ii) A velocity dependent effective angle is determined for the full range of velocities in the experiment. (iii) A full velocity vs. yaw-angle calibration using the method of Österlund (1999). It was found that the choice of method particularly affected the estimates of $w$.

## RESULTS AND DISCUSSION

### Calibration procedures

For the investigation of calibration procedures precise measurements of velocity and yaw-response of hot-wires had to be performed for velocities down to 0.5 m/s. Normally the velocity and yaw-response calibration of hot-wires are performed using a pitottube as reference at the centreline of the channel where the turbulence intensity is about 2-3 %. The wind tunnel cannot run at stable centreline velocities below 2 m/s and the use of pitottubes at such velocities is related to large measurement uncertainties. A specially designed calibration jet was therefore used for these calibrations. The round jet produces a flat-topped velocity profile with low turbulence intensity. The calibration rig was positioned on top of the channel and adjusted in angles so that the jet flow was coaxial to the channel flow. The traversing system can traverse the probes between the calibration rig and the channel flow, so the probes are never moved or disconnected between calibration and measurement.

Results show that the yaw response of a hot-wire is relatively stable for $\overline{U} > 6$ m/s, but that the effective angle decreases in an exponential manner with decreasing flow speeds (Fig. 1). This means that the concept of a fixed effective angle can be meaningful at relatively high velocities, but that the choice of angle becomes very subjective at low velocities. To check the importance of the choice of effective angle at low velocities, a test of the sensitivity of the mean and fluctuating velocities to a variation in the effective included angle was performed for a centreline velocity of 2 m/s (Table 1 corresponding to Fig. 2, only $\overline{v^{+2}}$ is shown). The three testcases defined in Table 1 gave no deviation in $\overline{U}$ and $\overline{u^{+2}}$, but substantial differences in $\overline{v^{+2}}$, $\overline{w^{+2}}$ and $\overline{u^+v^+}$. Since $\overline{u^{+2}}$ is not sensitive to a change in the effective angles, the distributions of $\overline{u^+v^+}$ are less sensitive than $\overline{v^{+2}}$. Using the method of a fixed effective angle, the effective angles are usually calculated at a velocity of $\sim$ 60 % of the centreline velocity to cover a wide range of velocities in the channel flow. This corresponds to Case 3 (○) in Fig. 2. Case 2 (△) and Case 1 (□) use the effective angles at 90 % and

Table 1: Cases for Fig. 2.

| Case | Symbol | Included angle [°] | Calibration Velocity [m/s] |
|---|---|---|---|
| 1 | □ | 61 | 2.0 |
| 2 | △ | 59 | 1.8 |
| 3 | ○ | 54 | 1.4 |

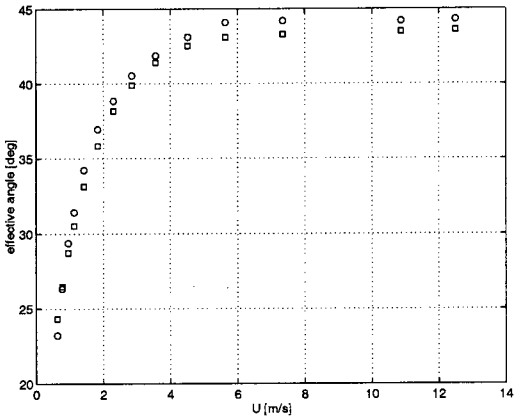


Figure 1: Effective angles for the wires of a UW-wire.

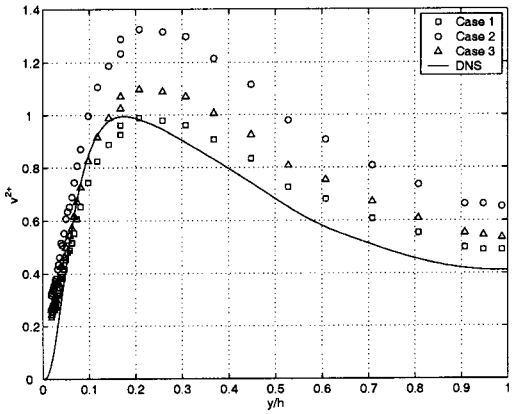


Figure 2: Test for the sensitivity of effective angles in $\overline{v^{+2}}$ at $\overline{U}_c \simeq 2m/s$. See Table 1 for symbols. Line: DNS, $Re \simeq 6500$ (Moser *et al.*, 1999)

100 % of the centreline velocity respectively. At $y/h = 0.3$ Cases 1,2 and 3 give a 7 %, 19 % and 44 % overshoot respectively compared to DNS (Moser *et al.*, 1999). It was therefore decided not to use the method of a single effective angle for low velocities. Snyder and Castro (1998) compared results from LDV with results from hot-wire experiments using a fixed effective angle and a velocity dependent effective angle showing promising results for the latter method. Limitations in their commercial software made it necessary to process the data using the effective angles appropriate to the indicated mean velocity only. A method using an effective angle dependent on the streamwise velocity on a sample-by-sample basis seemed more appropriate and was implemented here. The full velocity vs. yaw-angle calibration approach of Österlund (1999) and DNS of Moser *et al.* (1999) were used as reference. Österlund's method uses two 2-dimensional fifth order polynomials for the estimation of $U$ and $V$, where each polynomial uses both the sum and the difference of the voltages from the two wires as variables. Results from this method and the method of velocity dependent effective angles for $\overline{u^{+2}}$ and $\overline{v^{+2}}$ with an X-wire in the smooth channel showed excellent results compared to DNS. Problems with Österlund's method were encountered measuring $\overline{w^{+2}}$ in the smooth case and in the rough channel flow in general. Österlund used V-wire probes for measuring $\overline{w^{+2}}$, where the two wires are placed at $\pm$ 45° to the mean flow lying in the same horizontal plane. The spanwise extension is then considerable leading to poor spatial resolution approaching the wall. This is more serious in a rough case where the turbulence intensity is much higher than in the smooth case. A UW-probe similar to the one used for measuring $u$ and $v$, only rotated 90°, does not have the same problem with spatial resolution in the spanwise direction, but the effect of large $\frac{\partial u}{\partial y}$ approaching the wall is a problem for this kind of probe. Comparisons between the UW-, V-probe and DNS were made in the smooth channel flow and the UW-probe was found to give better results near the wall than the V-probe. Since the full velocity vs. yaw-angle method uses the sum and difference of the voltages from the two wires in the two calibration functions, a large part of the samples close to the wall must be discarded when using the UW-probe. The velocity dependent effective angle method, using a calibration function appropriate to each wire does not have this problem. Both methods gave very similar results for $\overline{w^{+2}}$ outside $y/h \simeq 0.2$ and compared very well with DNS (Moser *et al.*, 1999). A more important problem was encountered with the full velocity vs. yaw-angle method in the rough channel flow, since flow angles were substantially increased compared to the smooth channel case. Samples in the region close to the wall fell outside of the calibration area even though probes with included angles of 100° where used and the calibration was performed for yaw-angles of ±35°. The yaw-angle calibration area was limited to ±35° because at larger flow angles the calibration curves bended back into the region of calibration already spanned by points measured at smaller angles. This means that there is no one-to-one correspondence between the flow velocity and the voltage pair measured. One could argue that using probes with larger included angles would diminish this problem, but this would result in a poorer sensitivity of the lateral stresses. Outside $y/h \simeq 0.2$ all samples fell within the calibration region where the full velocity vs. yaw-angle method and the velocity dependent effective angle method gave almost identical results.

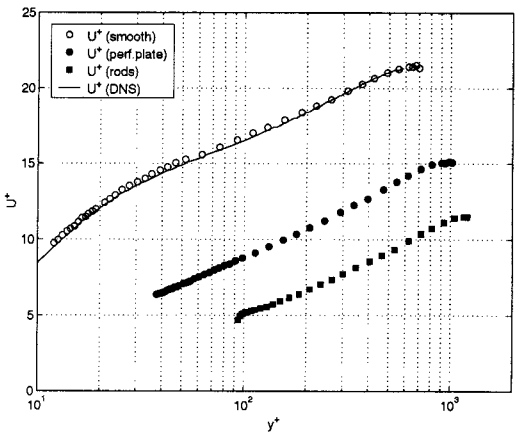


Figure 3: Mean velocity profiles, inner scaling.

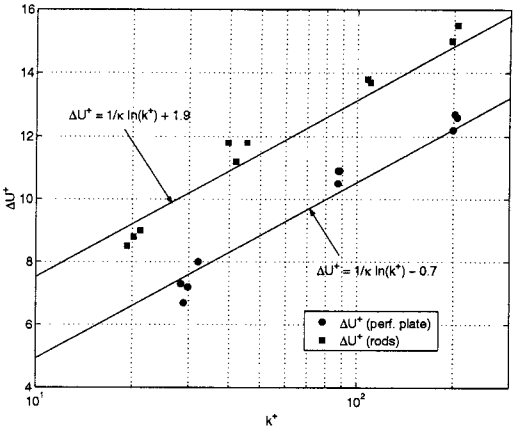


Figure 4: Mean velocity shift, $\Delta U^+$.

**Mean velocity**

$Re_\tau = hu_\tau/\nu$ for the smooth channel experiment was 670. The mean velocity profile for this case was found to match very closely the DNS data for $Re_\tau = 590$ (Moser *et al.*, 1999) above $y^+ \simeq 10$ (Fig. 3). Compared to the smooth reference case, the rough wall profiles ($Re_{\tau,rods} = 1230, Re_{\tau,perf.plate} = 940$) exhibit a downward shift in the log-law, $\Delta U^+$, as expected from classical theory (e.g. Townsend, 1976). $\Delta U^+$ was found to follow the characteristic logarithmic dependency with respect to $k^+$, consistent with a $k$-type behaviour (Fig. 4). It is evident from the figure that the roughness effect from the rod roughness is stronger than from the perforated plate. Calculations of the equivalent sand roughness, $k_s^+$, show that all $Re$ considered are in the fully rough regime ($k_s^+ > 70$). The error in origin, $\epsilon$, required in the case of a rough wall was determined using the semi-logarithmic form of the velocity distribution. Using the effective wall distance, $y_{eff} = y + \epsilon$, approximate similarity between the smooth and the rough surface flows is obtained in the velocity defect plot for both roughnesses (Fig. 5). Similarity in the outer layer suggests that the surface roughness effects are restricted to the inner wall layer.

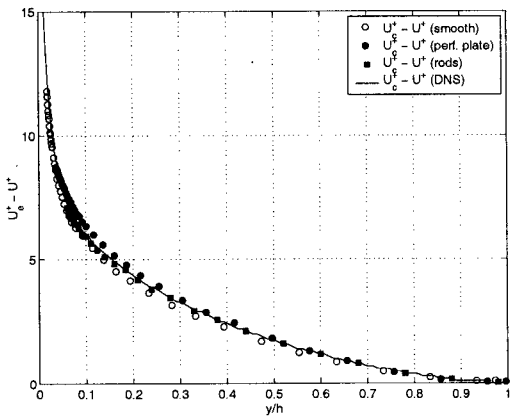


Figure 5: Velocity-defect profiles.

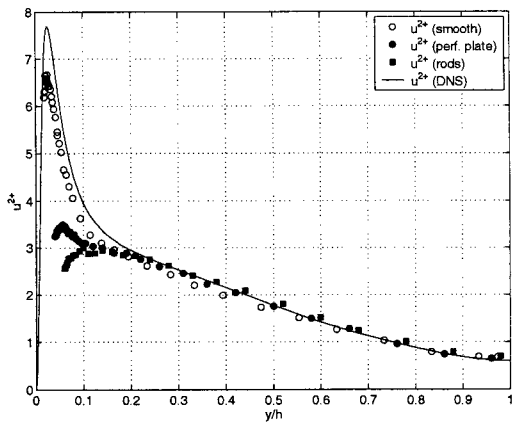


Figure 6: Normal stress $\overline{u^{2+}}$

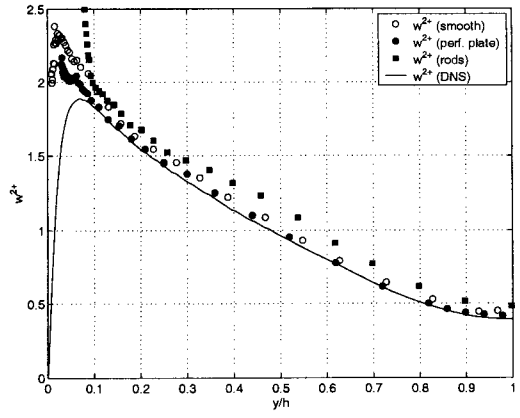


Figure 7: Normal stress $\overline{w^{2+}}$

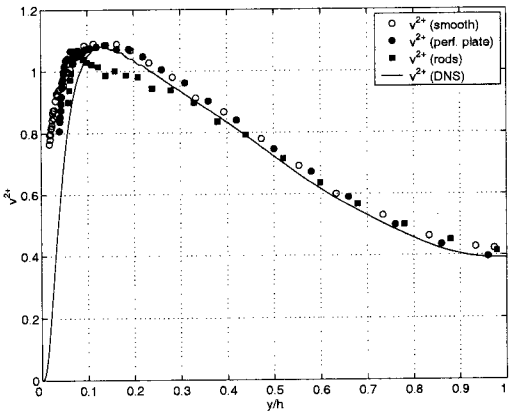


Figure 8: Normal stress $\overline{v^{2+}}$

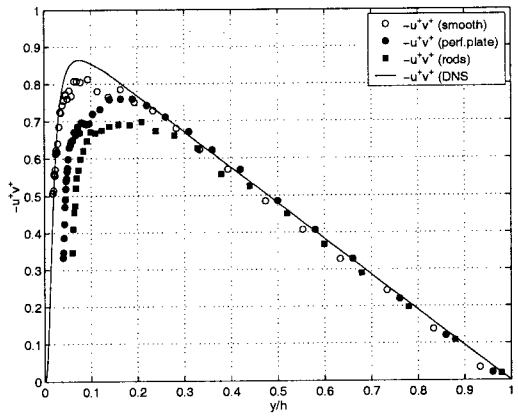


Figure 9: Shear stress $\overline{u^+v^+}$

**Reynolds stresses**

Reynolds stresses ($\overline{u^{+2}}, \overline{v^{+2}}, \overline{w^{+2}}, \overline{u^+v^+}$) are presented in Figs. 6 - 9. Within experimental uncertainty all $\overline{u^{+2}}$ profiles (Fig. 6) collapse onto a common curve outside $y/h \simeq 0.1$. This is consistent with Mazouz *et al.* (1998) for rod roughness in a channel flow and Sabot *et al.* (1977) for rod roughness in a pipe flow. Krogstad *et al.* (1992) found that the $\overline{u^{+2}}$ data over mesh roughness in a zero pressure gradient boundary layer were consistently slightly higher than over a smooth wall. This was attributed to the stronger wake in the rough case. Here the wake was found to be the same for all cases (Fig. 5). The collapse in $\overline{w^{+2}}$ profiles (Fig. 7) between the perforated plate and the smooth wall is very good. For the rod roughness slightly higher values for $\overline{w^{+2}}$ are observed. This may be caused by higher uncertainty in the estimation of $u_\tau$ for low $Re$ with the UW-wire as explained above. The increase in $\overline{w^{+2}}$ close to the wall appears to be unphysical and caused by high $\frac{\partial u}{\partial y}$, as suggested previously. The difference in $y/h$ values for this increase between the different surfaces is believed to be caused by increasing turbulence intensity from the smooth wall to the perforated plate to the rod roughness. Mazouz *et al.* (1998) found a substantial decrease for $\overline{w^{+2}}$ over the entire channel consistent with the findings of Sabot *et al.* (1977) for pipe flows. Both these investigations used considerably larger rods than in this experiment. The $\overline{v^{+2}}$ stresses (Fig. 8) for the perforated plate collapse onto the profile for the smooth channel for $y/h > 0.05$. For the rods a decrease is observed for $y/h < 0.3$, although never more than 10%. This applies to all $Re$ in the investigation. As for $\overline{w^{+2}}$, Mazouz *et al.* (1998) also found a substantial decrease in $\overline{v^{+2}}$ over the entire channel consistent with the observations of Sabot *et al.* (1977) for

a pipe. Krogstad *et al.* (1999) found large differences in the level for $\overline{v^{+2}}$ related to the wall geometry. The distribution of $\overline{v^{+2}}$ for the rod roughness was also very different from the other surfaces. Fig. 9 shows that for the shear stress, similarity is observed for the perforated plate and the smooth surface for $y/h > 0.2$, while for the rods the shear stress is considerably reduced for $y/h < 0.3$. The latter is believed to be a Reynolds number effect since the differences were found to be smaller for higher $Re$, but the decrease in level was always found to be present for $y/h < 0.2$. These results are consistent with Labraga *et al.* (1997) (experiments done under identical conditions as Mazouz *et al.*, 1998) who found only minor differences in $-\overline{u^+v^+}$ for the rough and smooth wall.

Differences observed between the rod roughness experiments of Mazouz *et al.* (1998), Sabot *et al.* (1977) and this experiment suggest that the size of the roughness elements is an important parameter. The strong effect of this type of roughness may imply that even in this study the size of the roughness elements is too large to be considered as simple perturbations to smooth channel flows. Results from the present study suggest that 2-D and 3-D roughness give different effects on the stresses. This is corroborated by Krogstad *et al.* (1999) from investigations in boundary layers. Comparisons with the latter investigation also suggest that the channel flow, where the turbulent flows at the two opposing walls interact, tends to produce roughness effects that differ in nature from that of the boundary layer.

## QUADRANT ANALYSIS

After observing a high degree of similarity between the flows over rough and smooth walls in the Reynolds stresses, especially for the perforated plate, it can be of interest to look for possible differences in the turbulent structures. Quadrant analysis (see Lu and Wilmarth, 1973) has proven to be a useful tool in assessing structural changes in turbulence. In the $u - v$ plane, the shear stress $uv = const.$ defines a hyperbola in two antisymmetric quadrants. Hence a triggering function $| uv | \geq Hu'v'$, where the prime denotes a r.m.s. value and $H$ is a threshold level, excludes shear stresses within a "hyperbolic hole". The contribution to $\overline{uv}$ from a particular quadrant, $Q$, may then be written

$$(\overline{uv})_Q = \lim_{T\to\infty} \frac{1}{T} \int_0^T uv(t)\, I_Q(t)\, dt\,. \qquad (1)$$

Here $I_Q(t)$ is the trigger function defined as

$$I_Q = \begin{cases} 1 & \text{when } | uv |_Q \geq Hu'v' \\ 0 & \text{otherwise.} \end{cases} \qquad (2)$$

It is worth noticing that an instantaneous motion with a large value of $u$ and small $v$ may contribute to $(\overline{uv})_Q$ in the same way as an event with small $u$ and high $v$, although the types of motion will be very different. Hence the quadrant method alone can not be used to uniquely distinguish contributions from a particular type of motion.

The shear stress signal is characterised by strong intermittency, where the main contributions to the averaged stresses come from large excursions in the second and fourth quadrants. When all events are included ($H = 0$), Fig. 10 shows that $Q2$ and $Q4$ both contribute between 60 and 80 % of $\overline{uv}$ throughout most of the channel flow. The results from the smooth surface compare very well with DNS (Moser *et al.*, 1999). The overshoot is compensated by small negative contributions from $Q1$ and $Q3$ which are very similar in magnitude (not shown). The distributions for the three

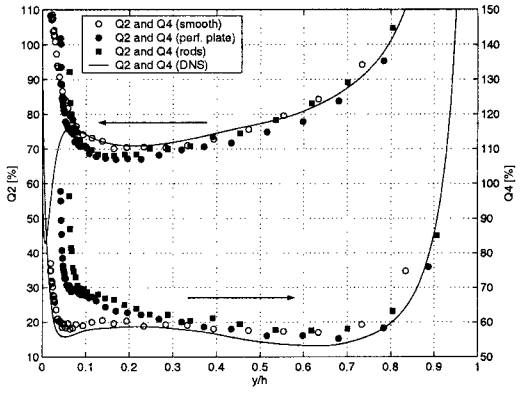


Figure 10: Contributions from Q2 and Q4 for H=0

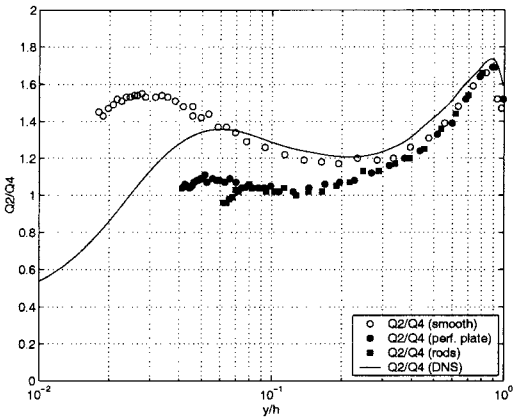


Figure 11: Ratio between Q2 and Q4 contributions for H=0

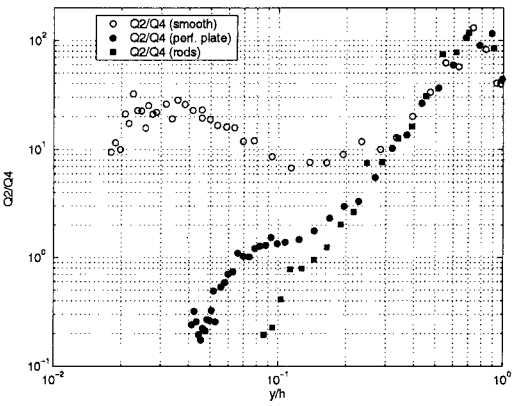


Figure 12: Ratio between Q2 and Q4 contributions for H=5

surfaces are very similar for most of the channel. Very near the wall $y/h < 0.1$, all contributions have a substantial rise which occurs somewhat further out in the rough cases. This is because the measurements in the rough cases were all taken above the roughness elements. A decrease in $Q2$ for $0.05 < y/h < 0.3$ can be seen for both rough surfaces. Grass (1971) argued that fluid trapped between the roughness elements as well as fluid from the viscous sublayer in the smooth case form a reservoir of low momentum fluid for the ejection

phase. The decrease in $Q2$ for the rough surfaces implies that the roughness elements act as inhibitors in the ejection phase compared to the smooth wall. This effect appears to be independent of the roughness geometry. It is therefore tempting to attribute this effect to small scale type motion. The increase in $Q4$ contribution over the rough surfaces is much more pronounced in the same region. These effects are even clearer in Fig. 11, where $\alpha = Q2/Q4$ is plotted for H=0. Notice that the wall region is enhanced by using a logarithmic abscissa. This ratio is the same for the three flows above $y/h \approx 0.3$, but near the surface the $Q4$ events become increasingly important in the rough cases, while $Q2$ events dominate for the smooth surface. This trend becomes even more obvious as the threshold level is increased (Fig. 12) For $H = 5$ (which corresponds to contributions only from events which are about 12 times stronger than $\overline{uv}$), the $Q2$ events are seen to dominate the entire flow field for the smooth wall, while $Q4$ becomes increasingly important for the rough surface for $y/h < 0.3$. An interesting feature of these figures is that although there is an important difference between the $-\overline{u^+v^+}$ distributions of the two rough surfaces for $y/h < 0.3$, their $Q4$ and $\alpha$ distributions collapse completely for $H = 0$ for $y/h > 0.07$. Only for very strong events, $H = 5$, there are differences between the two rough surfaces extending out to $y/h \simeq 0.2$, which is closer to the effects observed from the $\overline{u^+v^+}$ distributions. The main difference for $H = 5$ comes from the $Q2$ contribution (not shown), which implies that the rod roughness acts as a better inhibitor for very strong ejections compared to the perforated plate. The observation that the relative importance of sweep and ejection contributions are reversed in the rough wall flows compared with the smooth wall flow is consistent with the findings of Song and Eaton (2002) in a boundary layer with sand grain roughness and with Krogstad and Antonia (1999) in a boundary layer with rod roughness. These results corroborate the findings of Krogstad and Antonia (1999) that the main effect of the surface roughness is a reduction of the damping of $v$ motions as the wall is approached. Although the effect of roughness on the Reynolds stresses seem to be limited, the quadrant analysis also confirms the speculations of Krogstad *et al.* (1992) that surface roughness does not simply cause a modification of the wall boundary conditon, but affects the turbulence structure over a considerable part of the outer layer as well.

## CONCLUSION

A new calibration method for X-wires using velocity dependent effective angles is presented and validated against DNS (Moser *et al.*, 1999) and the state-of-the-art full velocity vs. yaw-angle method of Österlund (1999). Investigations at low velocities show that the effective angle is extremely sensitive to the velocity at which the calibration is performed and that lateral Reynolds stresses are extremely sensitive to the choice of effective angle. The new approach which lets the effective angle vary on a sample-to-sample basis significantly improves estimates of the Reynolds stresses at low velocities compared with the method assuming a fixed effective angle.

Measurements of five of the Reynolds stresses in a channel flow where the surfaces were roughened by means of square transverse rods and perforated plates showed that the stresses are affected beyond the immediate wall region only for the rods. Although the mean velocity defect for the rough walls and reference data taken in the same channel under smooth wall conditions were found to be very similar, differences in the stresses for the rods were found to extend to almost 10 roughness heights. This is at variance with conventional rough wall hypotheses which assume that the roughness effect is primarily a modification in the wall boundary condition which mainly affects the flow in the immediate vicinity of the roughness elements.

A quadrant analysis showed that the sweep type events are strongly affected by the roughness and the ejection type events are affected to a lesser degree. This is consistent with previous speculations (Krogstad *et al.*, 1992) that a rough wall primarily affects the turbulent structure by reducing the damping of the wall perpendicular motion and breaking up the streamwise vortices. The first effect mainly enhances the intensity of the sweeps near the wall, while the second effect reduces the streamwise length scales, making the flow more isotropic. A comparison of the two rough surfaces showed that despite important differences in the shear stress distributions, the contributions to the different quadrants were very similar, suggesting modifications of transport processes compared to smooth wall flows common to rough surfaces.

## REFERENCES


Bakken, O.M., and Krogstad, P.-Å., (2001), "Quadrant analysis of rough and smooth surface channel flow", *Turbulence and Shear Flow Phenomena - 2*, Lindborg *et al.*, eds., Universitetsservice, Stockholm, Sweden, Vol. 1, pp. 335-340

Bradshaw, P., (1971), *An introduction to turbulence and its measurement*, Oxford: Pergamon Press

Furuya, Y., Miyata, M. and Fujita, H., (1976), "Turbulent boundary layer and flow resistance on plates roughened by wires", *J. Fluids Eng.*, **98**, pp. 635-644

Grass, A.J., (1971), "Structural features of turbulent flow over smooth and rough boundaries", *J. Fluid Mech.*, **50**, pp. 233-255

Krogstad, P.-Å., Antonia, R.A. and Browne, L.W.B., (1992), "Comparison between rough- and smooth-wall turbulent boundary layers", *J. Fluid Mech.*, **245**, pp. 599-617

Krogstad, P.-Å. and Antonia, R.A., (1999), "Surface roughness effects in turbulent boundary layers", *Exp. Fluids*, **27**, pp. 450-460

Lu, S.S., and Willmarth, W.W., (1973), "Measurements of the structure of the Reynolds stress in a turbulent boundary layer", *J. Fluid Mech.*, **60**, pp. 481-571

Mazouz, A., Labraga, L. and Tournier, C., (1998), "Anisotropy invariants of Reynolds stress tensor in a duct flow and turbulent boundary layer", *J. Fluids Eng.*, **120**, pp. 280-284

Moser, R.D., Kim, J., Mansour, N.N., (1999), "Direct numerical simulation of turbulent channel flow up to $Re_\tau$=590", *Phys. Fluids*, **11**, pp. 943-945

Sabot, J., Saleh, I. and Compte-Bellot, G., (1977), "Effects of roughness on the intermittent maintenance of Reynolds shear stress in pipe flow", *Phys. Fluids*, **20**, 10, pp. S150-S155

Snyder, W.H. and Castro I.P., (1998), "The yaw response of hot-wire probes at ultra-low wind speeds", *Meas. Sci. Technol.*, **9**, pp. 1531-1536

Song, S. and Eaton, J.K., (2002), "The effects of wall roughness on the separated flow over a smoothly contoured ramp", *Exp. Fluids*, **33**, pp. 38-46

Townsend, A.A., (1976), *The structure of turbulent shear flow*, Cambridge University Press, Cambridge

Österlund, J.M., (1999), "Experimental studies of zero pressure-gradient turbulent boundary layer flow", Ph.D. Thesis, Royal Institute of Technology, Stockholm, Sweden